The Astrophysical Journal Letters, 891:L14 (6pp), 2020 March 1 https://doi.org/10.3847/2041-8213/ab77d0

Giant Planet Swaps during Close Stellar Encounters

Yi-Han Wang[1], Rosalba Perna[1,2], and Nathan W. C. Leigh[3,4]
[1] Department of Physics and Astronomy, Stony Brook University, Stony Brook, NY 11794, USA
[2] Center for Computational Astrophysics, Flatiron Institute, 162 5th Avenue, New York, NY 10010, USA
[3] Departamento de Astronomía, Facultad de Ciencias Físicas y Matemáticas, Universidad de Concepción, Concepción, Chile
[4] Department of Astrophysics, American Museum of Natural History, Central Park West and 79th Street, New York, NY 10024, USA
Received 2020 January 8; revised 2020 February 18; accepted 2020 February 19; published 2020 March 2

Abstract

The discovery of planetary systems outside of the solar system has challenged some of the tenets of planetary formation. Among the difficult-to-explain observations are systems with a giant planet orbiting a very low mass star, such as the recently discovered GJ 3512b planetary system, where a Jupiter-like planet orbits an M star in a tight and eccentric orbit. Systems such as this one are not predicted by the core accretion theory of planet formation. Here we suggest a novel mechanism, in which the giant planet is born around a more typical Sun-like star ($M_{*,1}$), but is subsequently exchanged during a dynamical interaction with a flyby low-mass star ($M_{*,2}$). We perform state-of-the-art N-body simulations with $M_{*,1} = 1M_{\odot}$ and $M_{*,2} = 0.1M_{\odot}$ to study the statistical outcomes of this interaction, and show that exchanges result in high eccentricities for the new orbit around the low-mass star, while about half of the outcomes result in tighter orbits than the planet had around its birth star. We numerically compute the cross section for planet exchange, and show that an upper limit for the probability per planetary system to have undergone such an event is $\Gamma \sim 4.4(M_{\rm c}/100M_{\odot})^{-2}(a_{\rm p}/{\rm au})(\sigma/1\ {\rm km\ s^{-1}})^{5}\ {\rm Gyr}^{-1}$, where $a_{\rm p}$ is the planet semimajor axis around the birth star, σ the velocity dispersion of the star cluster, and $M_{\rm c}$ the total mass of the star cluster. Hence these planet exchanges could be relatively common for stars born in open clusters and groups, should already be observed in the exoplanet database, and provide new avenues to create unexpected planetary architectures.

Unified Astronomy Thesaurus concepts: Exoplanet astronomy (486); Exoplanet dynamics (490); Stellar dynamics (1596); N-body simulations (1083)

1. Introduction

The discovery of several thousands of exoplanetary systems has clearly shown that planetary architectures are considerably more varied than originally thought (Batalha et al. 2013), and that planet formation models built to explain our own solar system fall often short of explaining features and patterns observed in other worlds.

Among the unexpected findings is the recent discovery of a giant planet orbiting a very low mass star (Morales et al. 2019), the M-dwarf GJ 3512b, with a mass of $0.12\,M_{\odot}$. The planet, of minimum mass $M_{\rm p}\sin = 0.463M_{\rm Jup}$, is on an eccentric (eccentricity $e = 0.435$) and tight orbit (semimajor axis $a_J = 0.338$ au).

The discovery of this system is not unique in the current exoplanet set: a giant planet of mass $M_{\rm p} = 0.63M_{\rm Jup}$ orbiting a very low mass host (a brown dwarf of mass $M = 0.06M_{\odot}$) was discovered in the microlensing event MOA-bin-29 (Kondo et al. 2019), and systems of this kind were reported since the early days of planet observations (Delfosse et al. 1998).

Planetary systems like these ones pose a serious challenge to the standard core accretion theory of planet formation (Mizuno 1980; Bodenheimer & Pollack 1986; Laughlin et al. 2004). It has in fact been shown (Laughlin et al. 2004) that the formation of Jupiter-mass planets orbiting M-dwarf stars is highly inhibited at all radial locations, in stark contrast to solar-type stars. More recent work (Miguel et al. 2020) further confirmed that in the planetesimal accretion scenario a system like GJ 3512b cannot be formed. Morales et al. (2019) further showed that the pebble accretion theory (Johansen et al. 2019) also fails in explaining the configuration of this planetary system. According to the pebble theory, giant planets accrete upon the formation of a core of at least 5 Earth masses. However, in a system with a low-mass star, migration is high and prevents the core to grow to much large sizes.

A possible explanation of systems like GJ 3512b, if its evolution has proceeded completely in isolation, involves the onset of the gravitational instability in the early phases of planet formation, when the protoplanetary disk was still relatively massive (Boss 2006; Morales et al. 2019). However, for typical values of the disk viscosity, fragmentation occurs in the outer parts of the disk, on the order of tens of au. Hence this model also requires substantial migration to have occurred. High eccentricities are not naturally predicted via this mechanism.

Here we propose a novel model to explain the properties of GJ 3512, motivated by the fact that many (if not most) stars are born within OB associations or in star clusters (e.g., Lada & Lada 2003). Even for the solar system, studies of the abundances of isotopes have led to the suggestion that it used to be part of a star cluster (Adams & Laughlin 2001). Clusters are generally thought to dissolve within 20–50 Myr; however, in the absence of external perturbations, they can be long-lived (de Grijs 2009), and in fact, long-lived clusters are known to exist (e.g., the Hyades and Presepe are about 600 Myr old, NGC 6811 is about 1 Gyr, NGC 6819 is about 2.5 Gyr, etc.; Meibom et al. 2015; Esselstein et al. 2018).

A number of studies (e.g., Heggie & Rasio 1996; Laughlin & Adams 1998; Bonnell et al. 2001; Davies & Sigurdsson 2001; Thies et al. 2005; Fregeau et al. 2006; Olczak et al. 2010; Chatterjee et al. 2012; Portegies Zwart & Jílková 2015; Cai et al. 2017, 2018; Rice et al. 2018; Cai et al. 2019; Flammini Dotti et al. 2019; van Elteren et al. 2019) have shown how the

evolution of planetary systems in interacting environments may provide alternative formation paths for planet properties that are difficult to account for by current theories of planetary formation. For example, internal dynamical interactions in multi-planet systems may have played a role in producing eccentric planetary orbits (e.g., Rasio & Ford 1996; Weidenschilling & Marzari 1996; de La Fuente Marcos & de La Fuente Marcos 1997; Chatterjee et al. 2008; Jurić & Tremaine 2008; Beaugé & Nesvorný 2012), in altering the distribution of mutual inclinations (Chatterjee et al. 2008; Boley et al. 2012), in shrinking the orbits of giants leading to hot Jupiters (e.g., Nagasawa et al. 2008; Shara et al. 2016; Hamers et al. 2017), or in creating free-floating planets (e.g., Chatterjee et al. 2008; Jurić & Tremaine 2008), which, upon capture, reside on very wide orbits (Perets & Kouwenhoven 2012).

Here we suggest a novel dynamical explanation to create a system such as GJ 3512b: the giant planet was originally born around a typical, Sun-like (G) star. However, during its lifetime, a flyby by a low-mass (M) star resulted in the planet being swapped between the two stars. Indeed, given the relatively high abundance of low-mass stars compared to solar-type ones (Miller & Scalo 1979), a scenario in which a "solar-type" planetary system is perturbed by a flyby of a low-mass star is the most common one to happen. We note that a planet exchange from a a main-sequence star to a neutron star–white dwarf binary system was suggested by Fregeau et al. (2006) to explain the planetary system PSR B1620-26.

We perform highly accurate N-body simulations to study the frequency of this planet exchange from the G to the M star, as well as the properties of the resulting planet and planet+star system. We find that, for stars born in associations, the rate of this special dynamical interaction is consistent with a handful of systems in the current exoplanet set. The high eccentricity is naturally explained via this mechanism, and tighter orbits than what the planet had around its birth star are found in about half of the exchanges.

Our Letter is organized as follows: Section 2 describes the computation of the cross section for the planet exchange, and hence the rate for this dynamical mechanism. We hence present (Section 3) the properties of the planetary system formed after the swap, and discuss them in the context of GJ 3512b. We summarize and conclude in Section 4.

2. Cross Section for Planet Exchange

The rate for planet exchange is given by

$$\Gamma_{\rm ex} \sim \sigma_{\rm ex} n_* \bar{v}, \tag{1}$$

where $\sigma_{\rm ex}$ is the cross section for this mechanism, n_* is the number density of stars in the environment under consideration, and $\bar{v}$ is the typical mean relative velocity in that environment.

In order to compute the cross section, we perform numerical scattering experiments with the very high precision few-body code `SpaceHub` (details in Wang et al. 2018, 2019). The code implements cutting-edge chain regularization (Mikkola & Aarseth 1993) and positive round-off error compensation in order to treat the high mass ratio of the star–planet systems that with traditional integrators often result in inaccurate results.

The cross section is calculated as a function of $M_{*,1}$, $M_{*,2}$, $M_{\rm p}$, $a_{\rm p}$, and V_∞, where $M_{*,1}$ is the mass of the G-type star that initially hosts the planet, $M_{*,2}$ is the mass of the M-type star

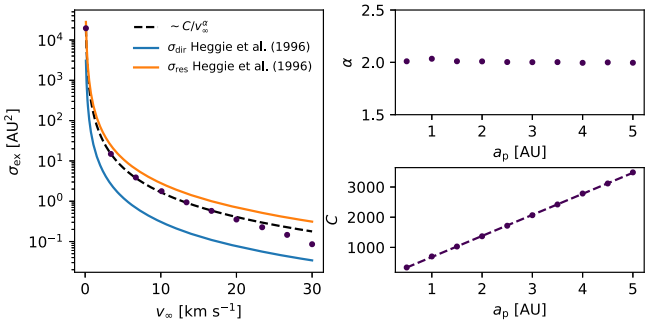

Figure 1. Results from numerical experiments and their best fit. Left: cross section for exchange of a giant planet from an 1 $M_\odot$ star to a 0.1 $M_\odot$ one, for an initial orbital separation $a_{\rm p} = 1$ au, which falls in the regime $v_{\rm c} < v_\infty < v_{\rm orb}$. As a reference, a comparison is made with the analytical formulas provided by Heggie et al. (1996) in the regime $v_\infty < v_{\rm c}$. Right: dependence of the cross section for exchange on the initial planet separation $a_{\rm p}$.

that dynamically interacts with the G star, $M_{\rm p}$ is the mass of the planet whose original semimajor axis is $a_{\rm p}$, and v_∞ is the relative velocity at infinity (prior to the scattering) between the center of mass of the G-type star–planet system and the M star.

For each set of values for $M_{*,1}$, $M_{*,2}$, $M_{\rm p}$, $a_{\rm p}$, and v_∞, we perform one million scattering experiments between the G-star/planet system and the flyby M star. The initial phase parameters of the planet orbit are isothermally distributed, i.e., $\cos(i)$ (i is the orbital inclination) is uniformly distributed within $[-1, 1]$, while Ω (longitude of the ascending node), ω (argument of periapsis), and the mean anomaly $\mathcal{M}$ are all uniformly distributed within $[-\pi, \pi]$. The impact parameter b is randomly generated from a distribution uniform in b^2 within the range $[0, b_{\rm max}]$. The maximum value $b_{\rm max}$, for each combination of $M_{*,1}$, $M_{*,2}$, $M_{\rm p}$, $a_{\rm p}$, and v_∞, is numerically predetermined to ensure that all the impact parameters $b < b_{\rm max}$ that may lead to planet exchange are included in the scattering experiment.

If $N_{\rm tot}$ is the total number of scattering experiments, and $N_{\rm ex}$ the number of outcomes found to be planet swaps, then the cross section for this mechanism is (e.g., Hut & Bahcall 1983)

$$\sigma_{\rm ex} = \pi b_{\rm max}^2 \frac{N_{\rm ex}}{N_{\rm tot}}, \tag{2}$$

with the statistical error

$$\Delta\sigma_{\rm ex} = \pi b_{\rm max}^2 \frac{\sqrt{N_{\rm ex}}}{N_{\rm tot}}. \tag{3}$$

In the following, in order to investigate planet swaps as a mechanism to explain systems such as GJ 3512, we specialize our simulations to the following values: $M_{*,1} = 1 M_\odot$, $M_{*,1} = 0.1 M_\odot$, and $M_{\rm p} = M_{\rm Jup}$, and explore the dependence on $a_{\rm p}$ (original orbital separation around $M_{*,1}$) and v_∞, since these are not directly measured variables.

The left panel of Figure 1 shows the cross section calculated from the scattering experiments as a function of v_∞ and for $a_{\rm p} = 1$ au. We parameterize our fit to these data as $\sigma_{\rm ex} = {\rm C}v^\alpha$, where C and α are fitting parameters. The best-fit power law to the numerical data is with $\alpha = -2.03$. The numerically derived cross section falls into the region between the cross section of direct planet exchange $\sigma_{\rm dir}$ in Equation (13) of Heggie et al. (1996), and the cross section of resonance planet exchange $\sigma_{\rm res}$ in Equation (15) of Heggie et al. (1996). In the Heggie et al. (1996) paper, the cross sections are estimated in the regime $v_\infty < v_{\rm c}$, where v_c is the critical velocity, i.e., the

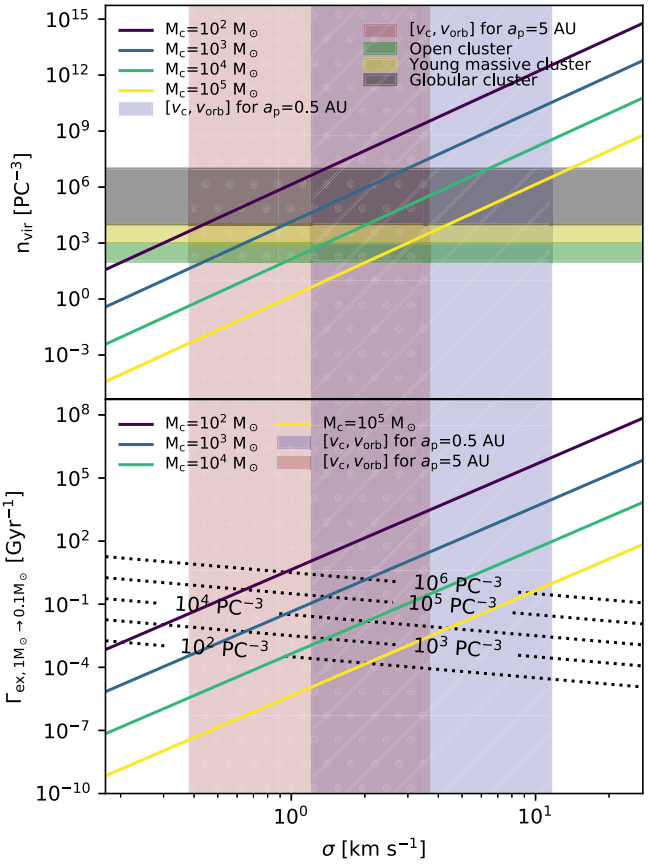

Figure 2. Upper panel: number density of virialized clusters as a function of σ. Bottom panel: rate of planet exchanges for virialized clusters, using the cross section in Figure 1. The dashed lines show the corresponding number densities.

velocity for which the total energy of the system is zero. However, most of the parameter space covered here is in the intermediate regime ($v_c < v_\infty < v_{orb}$), where v_{orb} is the initial orbital velocity of the planet. Thus, their regime does not directly apply to our calculations. This is also evident by the different behavior of the cross sections, which is shown for comparison in Figure 1. On the other hand, Fregeau et al. (2006) discussed the cross section of planet exchange in our regime. However, the cross section they provide for planet exchange is for the equal star mass case, unlike the low star mass ratio that we study here. The right panel of Figure 1 shows the linear relationship between a_p and σ_{ex} from the scattering experiments with different values of a_p.

For virialized clusters,

$$M_c \sim \frac{2R_c v^2}{G}, \tag{4}$$

where M_c and R_c are the mass and radius of the cluster, respectively, and v is its rms velocity. The number density of a virialized cluster can be then estimated as

$$n_{vir} \sim \frac{M_c/\bar{m}}{4\pi R_c^3/3} \sim \frac{6v^6}{\pi G^3 M_c^2 \bar{m}}, \tag{5}$$

where $\bar{m}$ is the mean stellar mass in the cluster. The upper panel of Figure 2 shows the number density of the virialized cluster with different cluster masses as a function of cluster velocity dispersion σ. The relationship between v_∞ and σ for a Maxwellian–Boltzmann distribution is

$$\sigma = \sqrt{\frac{3\pi - 8}{3\pi}}\, v, \ \langle v_\infty^2 \rangle = \langle 2v^2 \rangle. \tag{6}$$

Hence the exchange rate per planetary system can be estimated as

$$\Gamma_{ex} \sim n_{vir}\sigma_{ex} v \sim \frac{6\sigma_{ex} v^7}{\pi G^3 M_c^2 \bar{m}}. \tag{7}$$

Making use of the fitted σ_{ex}, and for a typical $\bar{m} = 0.5\ M_\odot$, we obtain

$$\Gamma_{ex,1M_\odot\to0.1M_\odot} \sim 4.4\left(\frac{a_p}{\mathrm{au}}\right)\left(\frac{\sigma}{\mathrm{km\ s^{-1}}}\right)^5\left(\frac{M_c}{10^2 M_\odot}\right)^{-2} \mathrm{Gyr^{-1}}. \tag{8}$$

The lower panel of Figure 2 shows the exchange rate (per planetary system) for $a_p = 1$ au and $\bar{m} = 0.5 M_\odot$ with different cluster masses. The dashed lines show the corresponding virialized number density, while the color regions indicate the interaction regime $v_c < v_\infty < v_{orb}$.

We need to point out that these rates should be considered as upper limits. First, the scattering experiments are made with a $1\ M_\odot$ star interacting with a $0.1\ M_\odot$ star. While these are indeed very common, the interacting stars have a mass distribution, upon which the cross section depends. Second, due to mass segregation, the more massive stars in a cluster will tend to sink toward the center, while the lighter G and M stars will populate the less dense regions of the cluster. Numerical simulations by Chatterjee et al. (2012) suggest that, due to primarily this reason, about 10% of all planetary systems around low-mass stars take part in a strong encounter in clusters similar to the open cluster NGC 6791.

Third (and most importantly), other dynamical processes, such as planet ejections, compete with planet exchanges during close encounters, and this is a sensitive function of environment. A full study of the relative rates of the various processes is deferred to follow-up work (Wang et al. 2020).

In the following, we will present the results of numerical experiments with three choices of the initial relative velocity: $v_\infty = 0.1$ km s^{-1} (for all a_p, in the hard binary regime where $v_\infty < v_c$), $v_\infty = 3.4$ km s^{-1} (for all a_p in the intermediate regime where $v_c < v_\infty < v_{orb}$), and $v_\infty = 13.4$ km s^{-1} (for $a_p = 5$ au, in the soft binary regime where $v_\infty > v_{orb}(5\ \mathrm{au})$). These fully bracket the typical values of stars born in dense groups (Binney & Tremaine 1987; Adams & Laughlin 2001).

3. Post-scattering Properties of the M-star/planet System

The orbital properties of the planet after being exchanged from the G to the M star are displayed in Figure 3. The left panel shows the 2D kernel density distribution of the post-scattered semimajor axis a_p' and eccentricity e_p' of the planet after the exchange, for a representative case with $a_p = 1$ au and $e_p = 0$. Along with the semimajor axis variation, the figure shows the intrinsic high eccentricity produced from the dynamical interaction. During a planet swap, the planet can be transferred from the original G star to the new M star in both prograde (M star flies by in the same direction of the planet orbit) and retrograde (M star flies by in the opposite direction to the planet orbit) orbits.

The right panels of Figure 3 show the collapsed (1D) probability distribution functions for a_p' (top panel) and e_p'

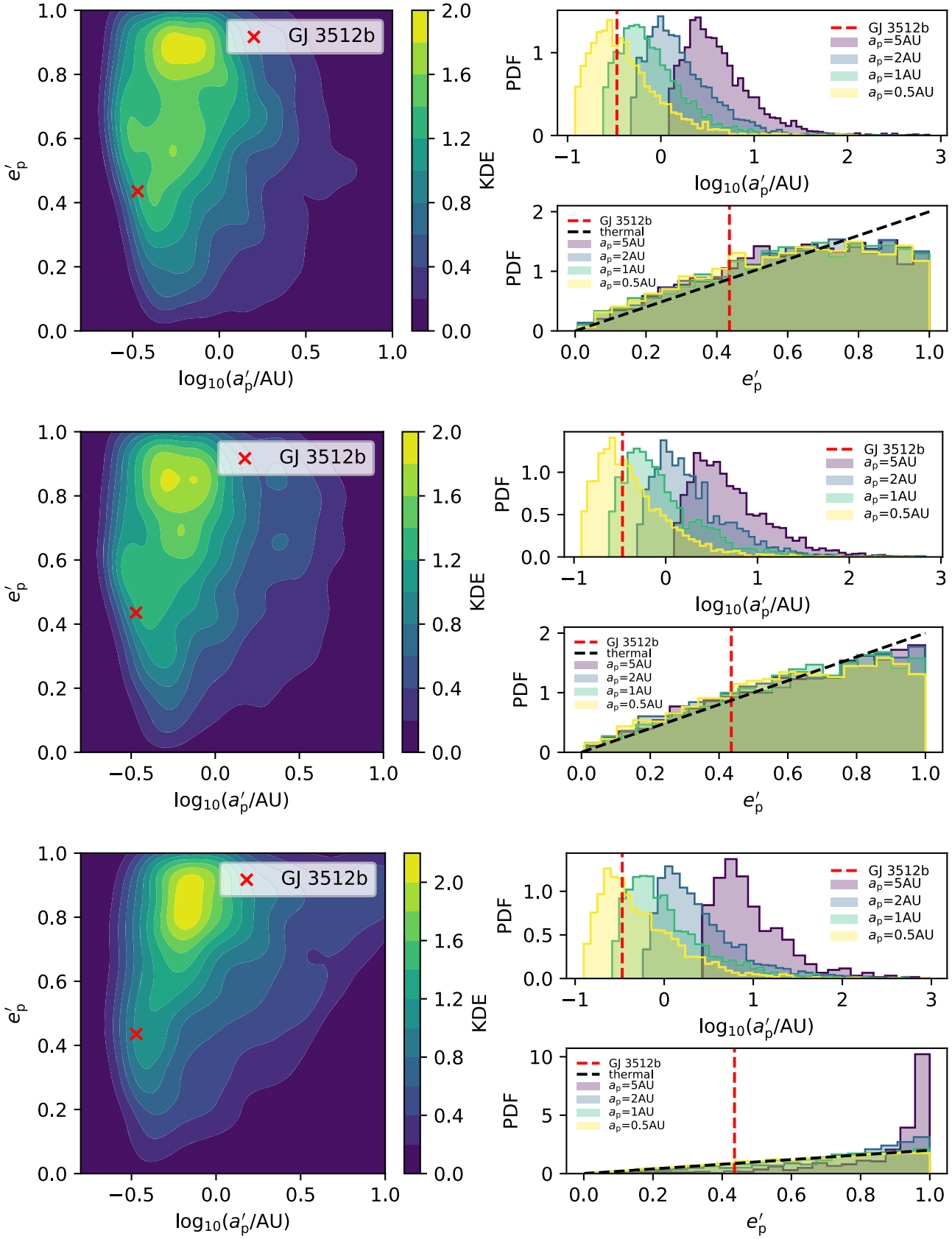

Figure 3. Post-scattering orbital separation and eccentricity of the planet after the swap onto the low-mass star, for three values of the relative velocity at infinity: $v_\infty = 0.1$ km s^{-1} (top panel), $v_\infty = 3.4$ km s^{-1} (middle panel), and $v_\infty = 13.4$ km s^{-1} (bottom panel). Left: 2D probability distribution function (PDF) for the case $a_p = 1$ au and $e_p = 0$. Right: the PDF of the orbital separation (top) and the eccentricity (bottom) for a range of a_p with $e_p = 0$. The observed parameters of GJ 3512b are also shown for reference.

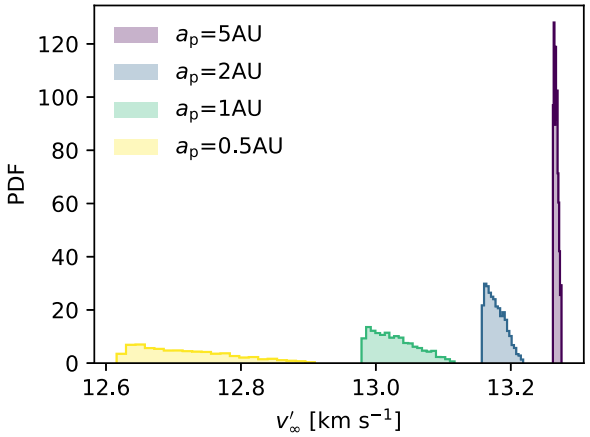

Figure 4. Post-scattering relative velocity of the M and G stars after the planet swap from the G to M star, for the case $v_\infty = 13.4$ km s^{-1}.

(bottom panel) for a range of initial orbital separations a_p of the planet, with $e_p = 0$ in all cases. In the hard binary regime ($v_\infty = 0.1$ km s^{-1}) where $v_\infty < v_c$, a'_p, on average, shifts toward the lower end as expected due to hardening. The shapes of the distributions for different a_p are almost identical. In this regime, e'_p is distributed more toward lower values compared with the thermal distribution. For different a_p, the distribution of e_p also looks similar.

To better interpret our results, we note that Hills & Dissly (1989) and Hills (1990) (see also Fregeau et al. 2006) found that, for extreme unequal mass scatterings, the hard/soft boundary is more accurately defined by v_{orb} rather than by v_c. Hence for intermediate regimes ($v_\infty = 3.4$ km s^{-1}) where $v_c < v_\infty < v_{orb}$, a'_p, on average, also becomes tighter. In this regime, the distribution of e'_p is almost thermal. For $a_p = 0.5$, 3.4 km s^{-1} is very close to its $v_c \sim 4.4$ km s^{-1}. Thus, the e'_p distribution displays the trend of shifting to the hard regime.

The case in the bottom panel of Figure 3, where $a_p = 5$ au and $v_\infty = 13.4$ km s^{-1}, is in the soft binary regime where $v_\infty > v_{orb}$. In this regime, we can see that a'_p, on average, shifts outward and the e'_p is distributed more toward high values compared to the thermal case.

The post-scattering relative velocity distribution of the two stars, after the M star has acquired the planet from the G star during the dynamical interaction, is shown in Figure 4 for the case $v_\infty = 13.4$ km s^{-1}. For this high relative velocity at infinity, the post-scattering relative velocity remains of the same order of magnitude as the initial one, showing only a slight decrease for tighter captures. The slight decrease comes from the binding energy shift. The average energy shift can be expressed as

$$\langle \Delta E \rangle \propto \frac{-M_{*2}}{\langle a'_p \rangle} - \frac{-M_{*1}}{\langle a_p \rangle} \propto \frac{M_{*1} - AM_{*2}}{\langle a_p \rangle}, \quad (9)$$

where $\langle a_p \rangle / \langle a'_p \rangle = A$ indicates the average semimajor axis shift with A almost identical for $a_p = 0.5$, 1, and 2 au. The shifted binding energy will boost/decelerate the center of mass velocity of the new M-star+planet system. For the specific setup studied here, as shown in the bottom right panel of Figure 3, we have $1 < A < 10$. With $M_{*1} = 1 M_\odot$ and $M_{*2} = 0.1 M_\odot$, this yields $\langle \Delta E \rangle > 0$. Due to energy conservation, the kinetic energy of the center of mass of the new star–planet system will decrease, which results in a reduction of v_∞.

As clearly shown in Equation (9), smaller a_p values yield larger energy shifts and a wider dispersion for the same values of $M_{*,1}$, $M_{*,2}$, and A.

For the two cases with smaller velocities ($v_\infty = 0.1$ and $v_\infty = 3.4$ km s^{-1}), the change in binding energy of the planet as it is swapped from the $1 M_\odot$ star to the $0.1 M_\odot$ flyby becomes comparable to or larger than the available kinetic energy in the system, and the two stars remain weakly bound (which is why we do not show their post-scattering relative velocity here). While we do not follow the long-term fate of these weakly bound stars (we are interested in the fate of the planet here), we note that in dense environments these binaries are likely to be eventually disrupted.

For a direct comparison with observations, we note that the velocity of the low-mass star is reflective of the post-scattering velocity only for a relatively short time. After the host cluster dissolution, the captured planetary system will end up orbiting as an isolated object within the host Galaxy potential. Hence the observed velocity of the star will become on the order of the orbital velocity of its original host cluster, imposing only very high relative velocity encounters with other isolated stars. Thus, the host cluster environment is, in our scenario, needed to ensure low relative velocity interactions, drastically increasing the capture probability per interaction.

4. Summary

Motivated by the discovery of planetary systems with gas giants orbiting low-mass stars, which are not explained by standard planet formation theories, here we have proposed a novel scenario of a dynamical origin: the giant is born around a more standard Sun-like star, but gets then captured by a low-mass star during a close encounter.

We have quantified the occurrence rate of these events, and the statistical properties of the post-scattered systems, via highly accurate direct N-body simulations, which yielded the (velocity-dependent) cross section for planet exchange. For small clusters with total mass $M_c \sim 10^2$–$10^3 M_\odot$ and velocity dispersion 1 km s^{-1} as typical of star clusters (Adams & Laughlin 2001), exchange rates can be as high as ~ 0.044–4.4 Gyr^{-1} per planetary system for a given planet-hosting Sun-like system and an interloper low-mass star, making this mechanism potentially relatively common for stars born in groups.

We find that, after the exchange, the distribution of planet eccentricity is weighed toward high values, whereas the orbital separation correlates with the initial one that the planet had around its host star, but the distribution is broad.

Our planet swap mechanism hence provides an alternative path to the formation of gas giants around very low mass stars, and naturally predicts some of the observed properties, such as the high orbital eccentricity.

We thank the referee for a very thoughtful and constructive report. N.W.C.L. acknowledges the generous support of Fondecyt Iniciacion Grant #11180005.

ORCID iDs

Yi-Han Wang https://orcid.org/0000-0002-8614-8721
Rosalba Perna https://orcid.org/0000-0002-3635-5677

References

Adams, F. C., & Laughlin, G. 2001, Icar, 150, 151
Batalha, N. M., Rowe, J. F., Bryson, S. T., et al. 2013, ApJS, 204, 24
Beaugé, C., & Nesvorný, D. 2012, ApJ, 751, 119
Binney, J., & Tremaine, S. 1987, Galactic Dynamics (Princeton, NJ: Princeton Univ. Press)
Bodenheimer, P., & Pollack, J. B. 1986, Icar, 67, 391
Boley, A. C., Payne, M. J., & Ford, E. B. 2012, ApJ, 754, 57
Bonnell, I. A., Smith, K. W., Davies, M. B., & Horne, K. 2001, MNRAS, 322, 859
Boss, A. P. 2006, ApJ, 643, 501
Cai, M. X., Kouwenhoven, M. B. N., Portegies Zwart, S. F., & Spurzem, R. 2017, MNRAS, 470, 4337
Cai, M. X., Portegies Zwart, S., Kouwenhoven, M. B. N., & Spurzem, R. 2019, MNRAS, 489, 4311
Cai, M. X., Portegies Zwart, S., & van Elteren, A. 2018, MNRAS, 474, 5114
Chatterjee, S., Ford, E. B., Geller, A. M., & Rasio, F. A. 2012, MNRAS, 427, 1587
Chatterjee, S., Ford, E. B., Matsumura, S., & Rasio, F. A. 2008, ApJ, 686, 580
Davies, M. B., & Sigurdsson, S. 2001, MNRAS, 324, 612
de Grijs, R. 2009, Ap&SS, 324, 283
de La Fuente Marcos, C., & de La Fuente Marcos, R. 1997, A&A, 326, L21
Delfosse, X., Forveille, T., Mayor, M., et al. 1998, A&A, 338, L67
Esselstein, R., Aigrain, S., Vanderburg, A., et al. 2018, ApJ, 859, 167
Flammini Dotti, F., Kouwenhoven, M. B. N., Cai, M. X., & Spurzem, R. 2019, MNRAS, 489, 2280
Fregeau, J. M., Chatterjee, S., & Rasio, F. A. 2006, ApJ, 640, 1086
Hamers, A. S., Antonini, F., Lithwick, Y., Perets, H. B., & Portegies Zwart, S. F. 2017, MNRAS, 464, 688
Heggie, D. C., Hut, P., & McMillan, S. L. W. 1996, ApJ, 467, 359
Heggie, D. C., & Rasio, F. A. 1996, MNRAS, 282, 1064
Hills, J. G. 1990, AJ, 99, 979
Hills, J. G., & Dissly, R. W. 1989, AJ, 98, 1069
Hut, P., & Bahcall, J. N. 1983, ApJ, 268, 319
Johansen, A., Ida, S., & Brasser, R. 2019, A&A, 622, A202
Jurić, M., & Tremaine, S. 2008, ApJ, 686, 603
Kondo, I., Sumi, T., Bennett, D. P., et al. 2019, AJ, 158, 224
Lada, C. J., & Lada, E. A. 2003, ARA&A, 41, 57
Laughlin, G., & Adams, F. C. 1998, ApJL, 508, L171
Laughlin, G., Bodenheimer, P., & Adams, F. C. 2004, ApJL, 612, L73
Meibom, S., Barnes, S. A., Platais, I., et al. 2015, Natur, 517, 589
Miguel, Y., Cridland, A., Ormel, C. W., Fortney, J. J., & Ida, S. 2020, MNRAS, 491, 1998
Mikkola, S., & Aarseth, S. J. 1993, CeMDA, 57, 439
Miller, G. E., & Scalo, J. M. 1979, ApJS, 41, 513
Mizuno, H. 1980, PThPh, 64, 544
Morales, J. C., Mustill, A. J., Ribas, I., et al. 2019, Sci, 365, 1441
Nagasawa, M., Ida, S., & Bessho, T. 2008, ApJ, 678, 498
Olczak, C., Pfalzner, S., & Eckart, A. 2010, A&A, 509, A63
Perets, H. B., & Kouwenhoven, M. B. N. 2012, ApJ, 750, 83
Portegies Zwart, S. F., & Jílková, L. 2015, MNRAS, 451, 144
Rasio, F. A., & Ford, E. B. 1996, Sci, 274, 954
Rice, D. R., Rasio, F. A., & Steffen, J. H. 2018, MNRAS, 481, 2205
Shara, M. M., Hurley, J. R., & Mardling, R. A. 2016, ApJ, 816, 59
Thies, I., Kroupa, P., & Theis, C. 2005, MNRAS, 364, 961
van Elteren, A., Portegies Zwart, S., Pelupessy, I., Cai, M. X., & McMillan, S. L. W. 2019, A&A, 624, A120
Wang, Y.-H., Leigh, N., Yuan, Y.-F., & Perna, R. 2018, MNRAS, 475, 4595
Wang, Y.-H., Leigh, N. W. C., Sesana, A., & Perna, R. 2019, MNRAS, 490, 2627
Wang, Y.-H., Perna, R., & Leigh, W. C. 2020, MNRAS, submitted (arXiv:2002.05727)
Weidenschilling, S. J., & Marzari, F. 1996, Natur, 384, 619